Characterization of nanoscale electronic structure in nonpolar GaN using scanning capacitance microscopy

J. J. M. Law and E. T. Yu[a)]
Department of Electrical and Computer Engineering, University of California, San Diego, La Jolla, California 92093-0407, USA

B. A. Haskell,[b)] P. T. Fini,[b)] S. Nakamura, J. S. Speck, and S. P. DenBaars
NICP-ERATO and Materials Department, University of California, Santa Barbara, Santa Barbara, California 93106-5050, USA

Scanning capacitance microscopy is used to characterize nanoscale, local electronic structure in nonpolar *n*-type GaN grown in the *a*-plane orientation using lateral epitaxial overgrowth (LEO). Analysis of the bias dependence of the scanning capacitance image contrast observed reveals the presence of a linear, positively charged feature aligned along the $[\bar{1}100]$ direction, extending from an LEO window region into the adjacent wing region and terminating a few microns into the wing region. Comparison of the scanning capacitance images with cathodoluminescence and transmission electron microscopy data, revealing the presence of line defects aligned along the $[\bar{1}100]$ direction that emerge from the window regions, indicates that this positively charged feature likely corresponds to a partial dislocation at the edge of a stacking fault. The observation of positive dislocation charge is striking in that studies of GaN grown in the polar *c*-plane orientation have predominantly revealed the presence only of negatively charged or electrically neutral dislocations. © 2008 American Institute of Physics. [DOI: 10.1063/1.2828161]

I. INTRODUCTION

Group III-nitride semiconductor materials and devices have emerged as outstanding candidates for a broad range of device applications, with particular success thus far in blue and ultraviolet light-emitting diodes[1] and laser diodes.[2] The spontaneous and piezoelectric polarization fields present in nitride heterostructures,[3] while typically being advantageous[4,5] in electronic devices such as nitride-based field effect transistors, can detract from the performance of light emitters based on nitride quantum-well structures due to the built-in electric field created within the quantum well by the polarization-induced charges at the heterojunction interfaces. Specifically, the built-in electric field leads to reduced electron-hole wave function overlap, and hence lower radiative recombination efficiency within the quantum well,[6] and in addition shifts light emission to longer wavelengths relative to polarization-free heterostructures.[7,8]

One possible method to address this issue entails the growth of nitride semiconductor heterostructure thin films in the so-called nonpolar orientations, e.g., on the $(10\bar{1}0)$ or $(11\bar{2}0)$ plane, referred to as the *m* plane and *a* plane, respectively, of the wurtzite crystal structure, rather than on the (0001) *c* plane as is most typically done. Indeed, growth and luminescence studies have shown that $In_yGa_{1-y}N/GaN$ quantum-well structures are free of such polarization-induced internal electric fields when grown in the *m*-plane[9] or *a*-plane[10,11] orientation. However, the continuing need to perform growth of nitride semiconductors on lattice-mismatched substrates such as sapphire or SiC leads to the presence of high densities of threading dislocations and other linear or planar defects, many of which can exhibit prominent electrical activity.[12–17] Because the densities and types of such defects, as well as their electrical behavior, can be highly dependent on growth conditions and technique, characterization of the electronic properties of defects in nonpolar nitride films is likely to be essential to their successful application in devices.

We have used atomic force microscopy (AFM) and scanning capacitance microscopy (SCM) to perform detailed studies of the electronic properties, specifically local, nanoscale charge distributions, in *n*-type GaN grown in the *a*-plane orientation with lateral epitaxial overgrowth (LEO) employed to reduce overall dislocation density. AFM and SCM imagings reveal the presence of a linear feature aligned along the $[\bar{1}100]$ direction, exhibiting bias-dependent SCM contrast arising from an elevated local concentration of positive charge. Based on comparison of our SCM data and other experiments done on similar *a*-plane GaN, we hypothesize that this positive charge is possibly due to the presence of a series of dislocations, a single dislocation, or a partial dislocation at the edge of a stacking fault aligned along the $[\bar{1}100]$ direction near the sample surface. Defects of the same line direction have been observed using transmission electron microscopy (TEM) and cathodoluminescence (CL) in LEO and non-LEO *a*-plane GaN (Refs. 18 and 24) and concluded to be the termination of basal plane stacking faults, suggesting a similar structural origin for the feature we observe. The observation of positive line defect charge is in contrast to the

a)Electronic mail: ety@ece.ucsd.edu.
b)Present address: Inlustra Technologies, LLC, Santa Barbara, California, 93111.

electrical behavior of dislocations observed in *c*-plane GaN thin films, in which threading dislocations propagating along the [0001] direction are typically either neutral or negatively charged.[14,17,19]

II. EXPERIMENT

The samples characterized in these studies were grown by hydride vapor phase epitaxy (HVPE), with LEO employed to improve surface morphology and reduce defect density.[20] A 120 nm thick SiO_2 layer was deposited on an *r*-plane sapphire substrate, then patterned with an array of stripe openings 5 μm in thickness with a 20 μm period. The stripes were aligned along the [$\bar{1}$101] direction, approximately 45° between the *c* and *m* axes, which correspond to the [0001] and [$\bar{1}$100] directions, respectively. A 105 μm thick GaN film was then grown through the windows in the mask layer. The sapphire substrate was removed through an *in situ* spontaneous film separation process. The resulting free-standing GaN film was unintentionally doped, resulting in *n*-type conductivity with a carrier concentration in the high 10^{17} cm^{-3} range.

For fabrication of ohmic contacts, samples were first rinsed and sonicated for 1 min in trichloroethylene, followed by rinsing and sonication in methanol, acetone, and isopropanol, and then cleaning in an oxygen plasma for 5 min. Ohmic contacts were then formed using 330 Å Ti/770 Å Al/330 Å Ti/880 Å Au metallization deposited by electron-beam evaporation and annealed at 400 °C for 5 min and then 650 °C for 3 min in a H_2/N_2 forming gas ambient. Prior to scanning probe characterization, samples were again cleaned using the procedure described above. AFM and SCM data were obtained using a Digital Instruments (Veeco) Nanoscope IIIa Dimension 3100 microscope with Pt/Ir-coated probe tips with a nominal radius of 25 nm at the tip apex. For the SCM measurements, a bias voltage consisting of a dc component with a small ($\sim$2 V) ac modulation, typically at a frequency of 20–95 kHz, was applied to the sample with the probe tip grounded. As discussed in detail elsewhere,[21–23] the SCM signal detection mechanism yields a voltage signal that is proportional, in our measurements, to dC/dV, where C is the tip-sample capacitance and V is the dc component of the applied bias voltage. Typical ambient conditions for these measurements were $\sim$20 °C and $\sim$50% relative humidity. Figure 1 shows a schematic diagram of the sample and probe tip geometry employed in these measurements.

III. RESULTS

Figure 2(a) shows a montage of AFM topographs of the sample near the border between a window region (the upper left portion of the montage) and an adjacent wing region (lower right). The crystal axis directions shown in the figure were determined by analysis of several large, distinctive pyramidal depressions observable in large-area surface topographs (not shown), whose facets are formed by (0$\bar{1}$12), ($\bar{1}$012), (01$\bar{1}$1), and (10$\bar{1}$1) crystal planes.[24] By determining the angle formed between each facet and the sample surface, each facet plane could be identified and the crystal axis di-
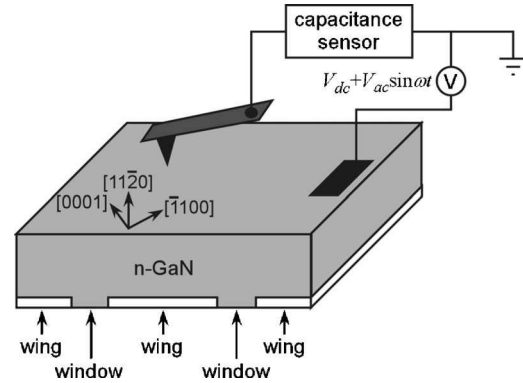

FIG. 1. Schematic diagram of sample structure, scanning probe measurement geometry, and voltage biasing arrangement.

rections determined. For ease of interpretation in terms of the analogous behavior of a conventional metal-insulator-semiconductor structure, for which it is typical to specify the voltage applied to the metal contact relative to the semiconductor, we at this point adopt the convention of specifying the potential of the probe tip relative to the sample in discussion and analysis of the SCM image data. Figures 2(b)–2(f) show the SCM images of the area, or portions thereof, corresponding to the topographic image in Fig. 2(a), obtained at dc bias voltages of +4 to −4 V applied to the tip relative to the grounded sample.

At a tip dc bias voltage $V_{tip} = +4$ V, we expect that an electron accumulation layer is formed at the surface so that any subsurface electronic structure is not imaged, as is evident from the absence of contrast in Fig. 2(b). As V_{tip} is decreased, the electron accumulation layer is gradually depleted and the tip-sample capacitance decreases. The resulting increase in dC/dV_{tip} increases the SCM signal level and
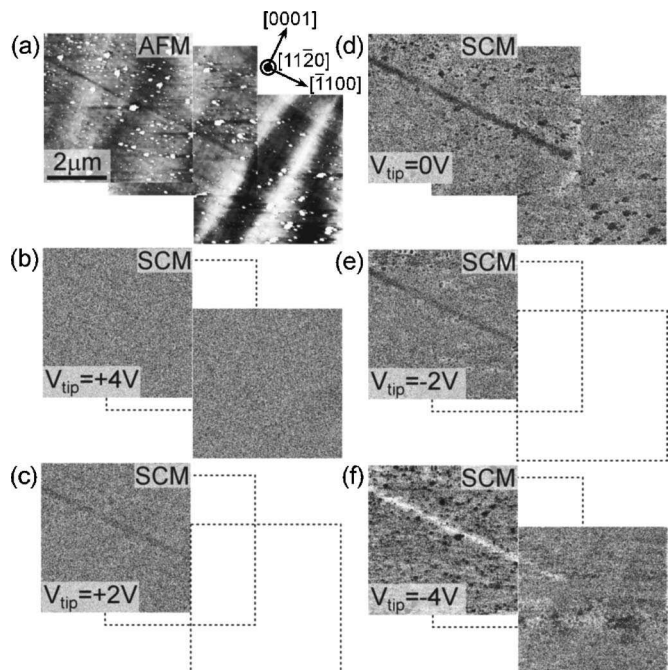

FIG. 2. (a) AFM topograph and [(b)–(f)] SCM images obtained at tip dc bias voltages of +4, +2, 0, −2 V, and −4 V. Dashed lines indicate areas in the topographic montage of (a) for which SCM data are not shown.

enables inhomogeneities in charge distribution within the surface depletion layer to be imaged. For $V_{tip}=+2$ V, we see in Fig. 2(c) that a linear region with decreased SCM signal, corresponding to a smaller value of dC/dV_{tip} relative to the surrounding areas, becomes visible. This feature is more prominent in Fig. 2(d), obtained at a bias voltage $V_{tip}=0$ V. We also see in Fig. 2(d) that the region of decreased SCM signal either terminates or moves to a depth greater than that which the SCM measurement is capable of probing, toward the lower right portion of the image area. Based on the observation by electron microscopy that defects in these samples typically terminate after propagating a short distance into the wing region on a free surface such as a coalescence front or a pit sidewall, and the relatively uniform contrast observed by SCM along the length of the feature prior to its disappearance, we believe that termination of the feature is more likely than propagation to an increased depth to be responsible for its disappearance from the SCM image. Figure 2(e) shows the SCM image obtained with $V_{tip}=-2$ V, at which the region of decreased SCM signal is still evident, but less prominent than for $V_{tip}=0$ V. Finally, we see in Fig. 2(f) that for $V_{tip}=-4$ V, the SCM image contrast is inverted, i.e., the region that exhibited a lower SCM signal level at more positive values of V_{tip} yields a higher SCM signal at $V_{tip}=-4$ V.

The presence of SCM image contrast only for $V_{tip} \leqslant +2$ V, combined with the smooth evolution and inversion of contrast as V_{tip} is decreased, indicates that the features observed correspond to actual electronic structure within the sample rather than being topographically induced artifacts. The AFM topograph shown in Fig. 2(a) does contain an area that is alternately depressed (upper-left portion of the image) and elevated (lower-right portion of the image) topographically compared to the surrounding region and that corresponds in location to the electronic feature imaged by SCM, suggesting a structural origin to the electronic feature.

IV. DISCUSSION

The electrical properties giving rise to the SCM contrast observed in Fig. 2 can be determined by an analysis of the bias dependence of the SCM signal. Using the simple model of the tip-sample interface as a conventional, one-dimensional metal-insulator-semiconductor structure, we can compute the capacitance per unit area C as a function of tip voltage in the accumulation and depletion regimes and differentiate to obtain dC/dV_{tip}.[25] The presence of trapped charge in such a structure, and its effect on C and dC/dV_{tip}, can then be analyzed in the usual manner to determine the origin of the observed SCM contrast in terms of electrical charge present along the dislocation line. In the actual SCM experiment, the maxima in dC/dV_{tip} will be shifted in voltage and the width of the associated peak will be increased compared to their calculated values due to the effects of finite tip size on carrier modulation within the sample[26] and the possible presence of surface or interface charges between the probe tip and sample.

Figure 3 shows capacitance per unit area and dC/dV_{tip} for an *n*-GaN metal-insulator-semiconductor structure, com-
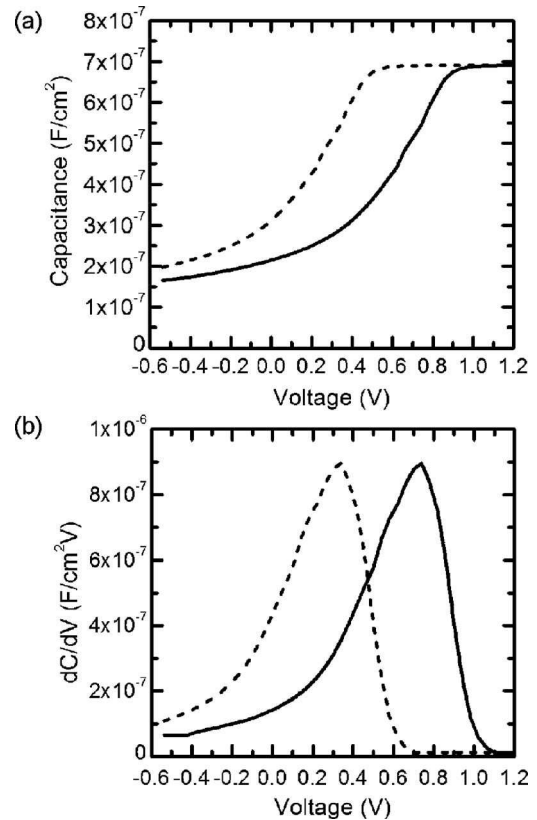

FIG. 3. (a) Capacitance per unit area C and (b) dC/dV_{tip} computed using a one-dimensional model for the metal tip, an electrically insulating layer between the tip and sample surface, and *n*-type GaN (solid lines), and the same structure with a positive sheet charge present immediately below the GaN surface (dashed lines).

puted in our model as a function of bias voltage applied to the metal, assuming a dopant concentration of 5×10^{17} cm^{-3}, an ideal metal-semiconductor barrier height of 0.8 eV, and the presence of an insulating layer separating the tip and GaN surface 5 nm in thickness with dielectric constant $3.9\varepsilon_0$. Also shown are capacitance and dC/dV_{tip} for the same structure in the presence of an additional, positive charge density $\Delta Q = 4 \times 10^{12}$ electron cm^{-2} just below the GaN surface, which shifts the voltage at which accumulation occurs by an amount $\Delta V \approx -\Delta Q/C_i$, where C_i is the capacitance per unit area of the insulating layer. This model is not, due to its extreme simplicity, expected to provide a quantitative description of the contrast observed in the SCM images shown in Fig. 2. It is, however, adequate to explain qualitatively the bias-dependent contrast observed in terms of additional charge density associated with the near-surface line defect present in the images.

Specifically, we see from Fig. 3(b) that a spatially localized shift in dC/dV_{tip}, i.e., the SCM signal level, induced by the presence of additional positive charge near the GaN sample surface, is expected to leave SCM signal contrast at large positive voltages unaffected, while yielding a depressed SCM signal level near the localized positive charge at lower voltages, with an eventual transition to elevated SCM signal levels near the localized positive charge as the voltage is further reduced. This is precisely the evolution in SCM contrast that is observed in the vicinity of the line defect imaged
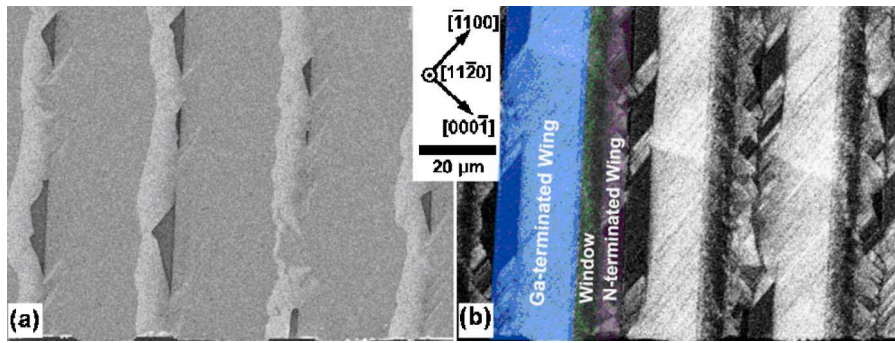
FIG. 4. (Color online) (a) Scanning electron micrograph and (b) polychromatic cathodoluminescence image of nonpolar LEO GaN sample revealing defects that act at nonradiative recombination centers aligned in the $[\bar{1}100]$ direction. Courtesy of Ref. 24.

in Fig. 2, indicating the presence of positive charge in or near the core of the defect. An analogous evolution of SCM signal contrast with bias voltage has been employed in earlier studies to identify the presence of negative charge associated with threading dislocations in *n*-type GaN and $Al_xGa_{1−x}N/GaN$ heterostructures grown in the *c*-plane (0001) orientation.[14,17,19]

In contrast to conventional thin film growth, the LEO growth procedure results in much more inhomogeneous spatial distributions of dislocations. Characterization by transmission electron microscopy (TEM) reveals very low dislocation densities, approximately 10^6 cm^{-2}, near the surface of the "wing" regions of the sample, while in the "window" regions the dislocation density typically exceeds 10^9 cm^{-2}. For *a*-plane LEO GaN films grown using $[1\bar{1}01]$-oriented stripes, dislocations typically emerge from the window regions and propagate at sharply inclined angles below the surface,[24] resulting in a very low dislocation density within the surface depletion layer—the region accessible for characterization of electronic structure by SCM. For the dopant concentrations present in the samples studied, the surface depletion layer under equilibrium conditions is expected to be 30–40 nm in thickness. However, TEM has also shown that stacking fault densities are comparable in wing and window regions.[24]

Figure 4 shows SEM and CL images of a sample grown in an identical manner to that employed in the present study, but with a 5 μm stripe opening and a 40 μm period to provide for increased lateral growth. These images reveal the presence of linelike regions of nonradiative recombination whose projection onto the surface is along the $[\bar{1}100]$. TEM analysis revealed that these features are the edges of basal plane stacking faults which terminate on partial edge dislocations.[18,24] The AFM image of Fig. 2(a) reveals the presence of an array of linear topographic features aligned along the $[\bar{1}100]$ direction with density comparable to that of the linear features observed by CL in Fig. 4. With regard to the SCM contrast shown in Fig. 2, it should be noted that both CL and TEM have a significantly larger penetration depth: several to tens of microns[27] and up to several hundred nanometers depending on sample thickness, respectively. In contrast, SCM is sensitive to features within the surface depletion layer—approximately 30–40 nm thick in this case. Thus, the apparent density of such features in an SCM image is expected, and found, to be much lower than in CL or TEM.

Given the one-dimensional nature of the feature we observed, its orientation along the same direction as that of the lines of nonradiative recombination observed by CL, and the prevalence of defects expected to be present within the surface depletion layer of the sample, we attribute the electronic structure we observe in Fig. 2 to the presence of a partial dislocation at the edge of a stacking fault. Comparing the CL and SCM findings, we note that in all cases the observed structure has the same line direction and similar dimensionality. Thus, it is likely that the defect observed SCM is a partial dislocation at the edge of a basal plane stacking fault.

The observation of a positively charged feature is striking in that prior studies of the electronic structure of threading dislocations in GaN grown in the *c*-plane orientation have revealed that those dislocations, typically propagating along the [0001] direction, are either negatively charged or electrically neutral, with the former behavior being associated with the presence of deep acceptor states within the dislocation core.[28,29] The defect structure we observe in these studies may therefore be of a type not previously characterized, but perhaps present in significant concentrations in GaN grown by LEO in nonpolar orientations.

V. CONCLUSIONS

In summary, we have used scanning capacitance microscopy to characterize local nanoscale electronic structure in free-standing, *a*-plane, *n*-type GaN grown by HVPE with LEO employed to reduce defect density. A linear feature containing positive charge is observed propagating from a window region into the adjacent wing region along the $[\bar{1}100]$ direction. This feature is present within the surface depletion layer in the sample, estimated to be approximately 30–40 nm in thickness, and appears to either terminate or move below the surface depletion layer within a few microns of the window edge. Cathodoluminescence data indicate that substantial concentrations of linear defects acting as nonradiative recombination centers are present in samples grown in this manner, and that these defects propagate along the $[\bar{1}100]$ direction as well. Transmission electron microscopy data show that the linear defects observable in cathodoluminescence are the terminations of basal plane stacking faults. On the basis of these observations and related studies of *a*-plane GaN, we interpret the electronic feature observed by SCM as being associated with a partial dislocation at the edge of a stacking fault. The observation of a positively charged linear defect in this material is significant in two

respects. First, it represents the first characterization of electronic structure associated with line defects in nonpolar GaN. Second, the observation of positive charge associated with the defect is quite striking, as linear defects such as threading dislocations in *c*-plane *n*-GaN are nearly universally observed to be either electrically neutral or negatively charged.

ACKNOWLEDGMENTS

[1] T. Nishida and N. Kobayashi, Phys. Status Solidi A **188**, 113 (2001).

[2] S. Nakamura, G. Fasol, and S. J. Pearton, *The Blue Laser Diode* (Springer, New York, 2000).

[3] O. Ambacher, J. Majewski, C. Miskys, A. Link, M. Hermann, M. Eickhoff, M. Stutzmann, F. Bernardini, V. Fiorentini, V. Tilak, B. Schaff, and L. F. Eastman, J. Phys.: Condens. Matter **14**, 3399 (2002).

[4] D. M. Asbeck, E. T. Yu, S. S. Lau, G. J. Sullivan, J. Van Hove, and J. M. Redwing, Electron. Lett. **33**, 1230 (1997).

[5] E. T. Yu, G. J. Sullivan, P. M. Asbeck, C. D. Wang, D. Qiao, and S. S. Lau, Appl. Phys. Lett. **71**, 2794 (1997).

[6] J. S. Im, H. Kollmer, J. Off, A. Sohmer, F. Scholz, and A. Hangleiter, Phys. Rev. B **57**, R9435 (1998).

[7] T. Takeuchi, S. Sota, M. Katsuragawa, M. Komori, H. Takeuchi, H. Amano, and I. Akasaki, Jpn. J. Appl. Phys., Part 2 **36**, L382 (1997).

[8] T. Deguchi, K. Sekiguchi, A. Nakamura, T. Sota, R. Matsuo, S. Chichibu, and S. Nakamura, Jpn. J. Appl. Phys., Part 2 **38**, L914 (1999).

[9] P. Waltereit, O. Brandt, A. Trampert, H. T. Grahn, J. Menniger, M. Ramseiner, M. Reiche, and K. H. Ploog, Nature (London) **406**, 865 (2000).

[10] M. D. Craven, P. Waltereit, F. Wu, J. S. Speck, and S. P. DenBaars, Jpn. J. Appl. Phys., Part 2 **42**, L235 (2003).

[11] H. M. Ng, Appl. Phys. Lett. **80**, 4369 (2002).

[12] H. M. Ng, D. Doppalapudi, T. D. Moustakas, N. G. Weimann, and L. F. Eastman, Appl. Phys. Lett. **73**, 821 (1998).

[13] T. Sugahara, H. Sato, M. Hao, Y. Naoi, S. Tottori, K. Yamashita, K. Nishino, L. T. Romano, and S. Sakai, Jpn. J. Appl. Phys., Part 2 **37**, L398 (1998).

[14] P. J. Hansen, Y. E. Strausser, A. N. Erickson, E. J. Tarsa, P. Kozodoy, E. G. Brazel, J. P. Ibbetson, U. Mishra, V. Narayanamurti, S. P. DenBaars, and J. S. Speck, Appl. Phys. Lett. **72**, 2247 (1998).

[15] J. W. Hsu, M. J. Manfra, R. J. Molnar, B. Heying, and J. S. Speck, Appl. Phys. Lett. **81**, 79 (2002).

[16] E. J. Miller, D. M. Schaadt, E. T. Yu, C. Poblenz, C. Elsass, and J. S. Speck, J. Appl. Phys. **91**, 9821 (2002).

[17] B. S. Simpkins, E. T. Yu, P. Waltereit, and J. S. Speck, J. Appl. Phys. **94**, 1448 (2003).

[18] R. Liu, A. Bell, F. A. Ponce, C. Q. Chen, J. W. Yang, and M. A. Khan, Appl. Phys. Lett. **86**, 21908 (2005).

[19] D. M. Schaadt, E. J. Miller, E. T. Yu, and J. M. Redwing, Appl. Phys. Lett. **78**, 88 (2001).

[20] B. A. Haskell, F. Wu, M. D. Craven, S. Matsuda, P. T. Fini, T. Fujii, K. Fujito, S. P. DenBaars, J. S. Speck, and S. Nakamura, Appl. Phys. Lett. **83**, 644 (2003).

[21] C. C. Williams, J. Slinkman, W. P. Hough, and H. K. Wickramasinghe, Appl. Phys. Lett. **55**, 1662 (1989).

[22] Y. Huang and C. C. Williams, J. Vac. Sci. Technol. B **12**, 369 (1994).

[23] D. M. Schaadt, E. J. Miller, E. T. Yu, and J. M. Redwing, J. Vac. Sci. Technol. B **19**, 1671 (2001).

[24] B. A. Haskell, "Structure of Nonpolar Gallium Nitride Films Grown by Hydride Vapor Phase Epitaxy," Ph.D. Dissertation, University of California, Santa Barbara, 2005.

[25] S. M. Sze, *Physics of Semiconductor Devices*, 2nd ed. (Wiley, New York, 1981), pp. 362–379.

[26] D. M. Schaadt and E. T. Yu, J. Vac. Sci. Technol. B **20**, 1671 (2002).

[27] B. G. Yacobi and D. B. Holt, *Cathodoluminescence Microscopy of Inorganic Solids* (Plenum, New York, 1990), pp. 57–119.

[28] A. F. Wright and U. Grossner, Appl. Phys. Lett. **73**, 2751 (1998).

[29] J. Elsner, R. Jones, M. I. Heggie, P. K. Stitch, M. Haugk, Th. Frauenheim, S. Öberg, and P. R. Briddon, Phys. Rev. B **58**, 12571 (1998).